Forkhead box F1 functions as a novel prognostic biomarker and induces caspase-dependent apoptosis in bladder cancer

YINING HAO, WEI HE, HAOFEI WANG, WENBIN RUI, FUKANG SUN, YU ZHU, DANFENG XU and CHENGHE WANG

Department of Urology, Ruijin Hospital, Shanghai Jiao Tong University School of Medicine, Shanghai 200025, P.R. China

Received April 24, 2023; Accepted July 18, 2023

DOI: 10.3892/or.2023.8610

Abstract. The downregulated expression of forkhead box F1 (FOXF1) has been found in many malignant tumors but no research was done in bladder cancer (BC). The present study aimed to investigate the prognostic value and antitumor effects of FOXF1 in patients with BC. Herein, a retrospectively recruited BC cohort and public datasets were utilized to identify the predictive ability of FOXF1 and determine its association with the clinical characteristics of BC patients. It was found that the expression level of FOXF1 was notably lower in BC tissues than in para-cancerous mucosae. Low FOXF1 expression was associated with unfavorable clinicopathological features and poor prognosis. Furthermore, in BC cells, the mRNA and protein expression levels of FOXF1 were examined using reverse transcription-quantitative PCR and western blot analysis. Cell viability was examined using Cell Counting Kit-8, EdU and clonogenic capacity assays. Cell apoptosis was detected using flow cytometry. The results revealed that the activation of FOXF1 impaired cell viability and induced apoptosis in BC. The antitumor effects of FOXF1 were also validated using animal models. Subsequently, caspase-3 was spotted as a downstream gene of FOXF1 by using RNA sequencing and protein-protein interaction analyses. FOXF1 inhibited proliferation and induced apoptosis of BC cells via caspase signaling pathway. The present study demonstrates the expression patterns, prognostic predictive ability and antitumor effects of FOXF1 in BC. FOXF1 is a favorable biomarker for predicting clinical outcomes in patients with BC and represents a potential therapeutic target.

Correspondence to: Professor Danfeng Xu or Professor Chenghe Wang, Department of Urology, Ruijin Hospital, Shanghai Jiao Tong University School of Medicine, 197 Ruijin Second Road, Shanghai 200025, P.R. China
E-mail: xdf12036@rjh.com.cn
E-mail: wch11971@rjh.com.cn

Abbreviations: BC, bladder cancer; MIBC, muscular invasive bladder cancer; NMIBC, non-muscular invasive bladder cancer; AJCC, American Joint Committee on Cancer; TCGA, The Cancer Genome Atlas; GEO, Gene Expression Omnibus; DEGs, differentially expressed genes; FC, fold change; OS, overall survival; IHC, immunohistochemistry; TNN, tumor node metastasis stage of tumors; FOXF1, forkhead box F1; RT-qPCR, reverse transcription-quantitative PCR; RNA-seq, RNA sequencing; PPI, protein-protein interaction

Key words: bladder cancer, forkhead box, biomarker, tumor suppressor gene, prognosis

Introduction

Bladder cancer (BC) is the 12th most common type of cancer worldwide, which imposes substantial financial burden to societies. According to the statistics, there were 573,278 new BC cases in 2020 worldwide (1). Of the BC cases, ~75% are non-muscle-invasive BC (NMIBC) and the remainder are muscle-invasive BC (MIBC). Currently, cystoscopy is the gold standard diagnostic procedure, and the American Joint Committee on Cancer (AJCC) TNM system is commonly used to predict the clinical outcomes of patients with BC (2,3). However, the individual genetic heterogeneity often results in divergent clinical outcomes, which stresses the vital necessity to identify biomarkers for BC.

With advancements being made in transcriptomics, a number of biomarkers for BC prognosis have emerged, such as urinary extracellular vesicles (4), telomerase reverse transcriptase promoter mutations (5) and nuclear matrix protein 22 (6). The forkhead box (FOX) superfamily consists of 43 evolutionarily conserved transcriptional regulators that participate in DNA repair, cell lineage, embryogenesis and longevity (7,8). The forkhead domain enables the combination of members with target DNA, and is responsible for their promotive or suppressive effects on gene transcription. A number of FOX members have been proven to be differentially expressed in various BC subtypes, and the dysregulation of FOX genes may be involved in bladder tumor development and progression (9,10).

As a transcription factor in the hedgehog signaling pathway (11), FOXF1 plays critical roles in gastrointestinal tract development, cancer-associated fibroblasts (12), endothelia progenitor activation (13) and VEGF signaling regulation (14). Recently, the effects of FOXF1 in the antitumor process and its association with the prognosis of patients have been demonstrated. In papillary thyroid cancer, hepatocellular carcinoma and lung adenocarcinoma, FOXF1 is downregulated in tumor

tissue compared with pericarcinomatous tissues; the decreased expression of FOXF1 has been found to be associated with more malignant phenotypes and a poorer survival, indicating its predictive ability in the prognosis of patients (15-17). However, the effects of FOXF1 in BC have not yet been fully elucidated.

The present study aimed to investigate the expression patterns of FOXF1 in BC, evaluate the association between FOXF1 expression levels and the clinicopathological features of patients with BC, and explore the antitumor mechanisms of FOXF1 in BC. The results described herein demonstrate that FOXF1 expression is downregulated in BC tissues, its activation inhibits cell proliferation and induces cell apoptosis via the caspase signaling pathway. The decreased expression level of FOXF1 is associated with a more severe clinical stage, muscle invasion, lymphatic infiltration and a poorer prognosis of patients with BC. The expression level of FOXF1 may thus have robust predictive ability in the clinical outcome of patients with BC.

Materials and methods

Patients and clinical information. The present study recruited 64 patients with BC undergoing cystectomy at Ruijin Hospital (Shanghai, China) between January, 2007 and February, 2022 (Ruijin Cohort). The present study was performed in accordance with the Declaration of Helsinki. The studies involving human participants were reviewed and approved by the Ethics Committee of Ruijin Hospital, School of Medicine, Shanghai Jiao Tong University (PA23030202). Informed consent was obtained from each patient. The patient specimens were pathologically diagnosed using three independent experts. The BC samples and matched normal bladder mucosae were embedded into a tissue microarray (Shanghai Outdo Biotech Co., Ltd.). Clinical and pathological data were recorded, including sample ID, age, sex, operation data, follow-up period, status, tumor grade, tumor size, metastatic lesion and lymphatic infiltration, followed by determining their stages according to the 8th AJCC staging system (18).

Data collection and preprocessing. Gene chips were first selected from the Gene Expression Omnibus (GEO) (https://www.ncbi.nlm.nih.gov/geo/). The inclusion criteria for validating the FOXF1 expression patterns are as follows: i) The biospecimens were obtained from human primary bladder cells or tissues; ii) transcriptomic data; iii) samples contained para-cancerous samples; iv) contained at least six samples in each group. In total, eight independent GEO datasets, GSE121711, GSE13507, GSE188715, GSE3167, GSE37815, GSE38264, GSE40355 and GSE42089 that met the requirements were collected using the 'GEOquery' package (19). The FOXF1 expression levels of pan-cancer tissues were acquired from the GEPIA1 website (http://gepia2.cancer-pku.cn/). Moreover, to validate the FOXF1 expression levels in different types of BC, the RNA sequencing (RNA-seq) data were downloaded and the clinical information of 411 patients with BC was obtained from The Cancer Genome Atlas (TCGA) database (https://portal.gdc.cancer.gov/).

The inclusion criteria for validating the prognostic predictive performance of FOXF1 are as described below: i) The biospecimens were obtained from human primary bladder cells or tissues; ii) transcriptomic data; iii) the survival information was available; iv) a sufficient sample size was included for survival analysis. Four independent GEO datasets (GSE31684, GSE48075, GSE169455 and GSE13507) and an immunotherapy cohort (IMvigor210) with their corresponding survival data were obtained from the GEO website, 'IMvigor210CoreBiologies' and 'IOBR' packages (20). The cut-off values for the FOXF1 expression level in these datasets were determined using 'X-tile' software (version 3.6.1; https://medicine.yale.edu/lab/rimm/research/software/).

Immunohistochemistry staining and scoring of FOXF1. Tissues were fixed with 4% paraformaldehyde for 48 h at room temperature, then paraffin-embedded and prepared into a tissue chip by Shanghai Outdo Biotech Co., Ltd. Immunohistochemistry (IHC) of the tissue microarray was performed using streptavidin-peroxidase methods. Specifically, the slides were deparaffinized with xylene for 30 min at room temperature followed by rehydration using a series of graded alcohols (100, 95, 80 and 70%, 5 min for each step, at room temperature). Heat-induced epitope retrieval (with Tris/EDTA pH 9.0 buffer) was then performed using a induction heater for 20 min at 60˚C. Non-specific binding sites were blocked using Immunol Staining Blocking Buffer (Beyotime Institute of Biotechnology) for 15 min at room temperature. Subsequently, the microarray was incubated with primary antibody against human FOXF1 (1:100 dilution; cat. no. PAB30083, Abnova) overnight at 4˚C. The following day, the microarray was washed with TBST (Wuhan Servicebio Technology Co., Ltd.) for 30 min at room temperature and incubated with the HRP-conjugated goat anti-rabbit lgG antibody (ready to use; cat. no. D110073, Sangon Biotech Co., Ltd.) for 1 h at room temperature. The slides were then stained using diaminobenzidine (Beyotime Institute of Biotechnology) for 5 min at room temperature and re-stained with hematoxylin (Beyotime Institute of Biotechnology) for 10 min at room temperature. Finaly, a series of graded alcohols (70, 80, 90 and 100%, 10 sec for each step, at room temperature) followed by xylene (10 sec, at room temperature) were used for dehydration of the tissues. The slides were mounted by neutral balsam (Wuhan Servicebio Technology Co., Ltd.) and scanned using Pannoramic MIDI automatic digital slide scanner (3DHISTECN Ltd.). The negative controls were treated using the same experimental process, but the primary antibody was rabbit IgG (1:200; cat. no. 30000-0-AP, Proteintech Group, Ltd.). Positive staining was considered when staining was predominantly located in the nucleus and cytoplasmic staining was regarded as non-specific staining. The expression level of FOXF1 was quantified by the proportion of positive cell nucleus and their staining intensity as follows:

$$H\text{-}score = \sum Staining\ intensity * Staining\ area\ persentage$$

The staining intensity was graded into four levels as follows: 0 (negative), 1 (weak), 2 (moderate) and 3 (strong); the staining area percentage was defined as the percentage of cell nucleus with a corresponding staining intensity (0-100). Three pathologists, who were blinded to the clinical information of the patients, scored the immunoreactivity of FOXF1

independently on an Aperio ImageScope (magnification, x400; Leica Microsystems GmbH); the final H-score was the average of their scores.

Evaluation of the prognostic predictive performance of FOXF1 expression. For the patients in TCGA dataset, their survival outcomes were compared with the aid of the KMplotter online database (https://kmplot.com/analysis/). For the patients in the GEO datasets and the IMvigor210 cohort, their survival information was acquired from the corresponding website. All patients in each dataset were divided into the FOXF1-high and FOXF1-low groups based on a cut-off value produced using X-tile' software. Survival risk differences between the two groups were determined using Kaplan-Meier survival analysis and the log-rank test. Univariable and multivariable Cox regression analyses were performed to examine the independency of FOXF1 in predicting the overall survival (OS) of patients with BC. Boxplots were used for revealing the association between FOXF1 expression and the clinicopathological features of the patients.

Cells, cell culture and chemical reagents. Human bladder cancer cell lines 5637 (HTB-9), J82 (HTB-1), T24 (HTB-4) and the normal uroepithelium cell line SV-HUC-1 (CRL-9520), were acquired from ATCC. The EJ cell line (YS1803C) was obtained and STR-authenticated by Shanghai Yaji Biological Technology Co., Ltd.. The SV-HUC-1 cells were cultured in Ham's F-12K medium (Gibco; Thermo Fisher Scientific, Inc.) supplemented with 10% fetal bovine serum (FBS, Gibco; Thermo Fisher Scientific, Inc.); the 5637, J82, EJ and T24 cells were cultured in RPMI-1640 medium (Gibco; Thermo Fisher Scientific, Inc.) supplemented with 10% FBS. All cells were cultured in humidified incubator with 5% CO_2 at 37˚C. Ac-DEVD-CHO (Beyotime Institute of Biotechnology) at a final concentration of 50 μM was used to inhibit caspase-3 activity 12 h after dsRNA transfection.

self-amplifying RNA (saRNA) design, transfection with double-stranded RNA (dsRNA) and infection with recombinant lentivirus. The promoter sequence (1 kb) of FOXF1 was downloaded from the National Center for Biotechnology Information (https://www.ncbi.nlm.nih.gov/gene/). An Excel macro template was used to read the promoter sequence and the putative saRNA target sites were scanned as previously described (21). Following manual screening, four saRNAs and a non-specific negative control (dsControl) were synthesized by GenePharma Co., Ltd.; the sequences of the five dsRNAs are listed in Table SI. Transfection with the dsRNAs (final concentration, 50 nM) was performed using Lipofectamine RNAiMax (Invitrogen; Thermo Fisher Scientific, Inc.) according to the manufacturer's instructions. RNA was isolated from the BC cells at 48 h following transfection, and total proteins were extracted from the BC cells at 72 h following transfection; the time durations between transfection and other phenotypic experiments are specified in the relevant subsections below.

The efficiencies of the four saRNAs were examined using reverse transcription-quantitative PCR (RT-qPCR) and western blot analysis. The most efficient saRNA and dsControl were selected to create short hairpin RNA (shDNA) and packaged into lentivirus (Lenti-dsFOXF1-367 or Lenti-dsControl, GenePharma Co., Ltd.). The cells were infected by the lentivirus at a confluency of 60-70%, and the medium was replaced 24 h later. Cells with the stable activation of FOXF1 were selected with 3 μg/ml puromycin (Beyotime Institute of Biotechnology).

RT-qPCR. Total RNA was isolated from the BC cells, carcinoma and adjacent tissue samples using TRIzol® reagent (Invitrogen; Thermo Fisher Scientific, Inc.). The reverse transcription of 1,000 ng RNA was carried out using the First Strand cDNA Synthesis kit (cat. no. D7178; Beyotime Institute of Biotechnology) according to the manufacturer's instructions, the reaction system was incubated for 30 min at 42˚C, then heated for 10 min at 80˚C. The gene expression level was detected using SYBR-Green qPCR Mix (cat. no. D7262; Beyotime Institute of Biotechnology) and quantified using the $2^{-\Delta\Delta Cq}$ method (22). GAPDH was used as the reference gene. Primers were produced by Biosune Biotechnology (Shanghai) Co.; their sequences are presented in Table SI.

RNA-seq and protein-protein interaction (PPI) network analysis. The RNA-seq library construction was completed by Shanghai Biotree Biotech Co., Ltd.. The negative control (nc) and FOXF1-activated (sa) group of BC cells were established, and the quantity and purity of the RNA were analyzed using a Bioanalyzer 2100 and RNA 6000 Nano LabChip kit (Agilent Technologies, Inc.). The mRNAs were purified using oligo $(dT)_{25}$ magnetic beads (Invitrogen; Thermo Fisher Scientific, Inc.), followed by fragmenting to ~200 bp (magnesium RNA fragmentation module, New England Biolabs) and reverse transcription (random hexamer priming method, Invitrogen; Thermo Fisher Scientific, Inc.). After adding A-base, ligating adaptor and PCR amplifying, the products libraries were sequenced on an Illumina platform (Novaseq™ 6000) in accordance with the vendor's recommended protocol.

Differentially expressed genes (DEGs) and PPI analysis. DEGs were identified based on a threshold set as fold change (FC) >2 or <0.5, and adjusted P-value <0.05. The PPI network was analyzed on the STRING website (https://cn.string-db.org/) and using Cytoscape software (version 3.9.1; https://cytoscape.org/); the degree of protein interaction was calculated using the maximum neighborhood component (MNC) method.

Western blot analysis. Total proteins were extracted from the BC cells using RIPA buffer (NCM Biotech) supplemented with protease inhibitor cocktail (NCM Biotech). The concentrations of the proteins were determined using the BCA method (Epizyme). The supernatants containing 30 μg protein were separated by 7.5% SDS-PAGE and then blotted onto PVDF membranes (MilliporeSigma). The membranes were incubated with 5% skim milk for 2 h at room temperature in order to block non-specific binding sites. After washing with TBST (Wuhan Servicebio Technology Co., Ltd.) for 10 min at room temperature, primary antibodies included FOXF1 (1:3,000 dilution; cat. no. ab168383, Abcam), Bax (1:1,000 dilution; cat. no. R22708), caspase-9 (1:1,000 dilution; cat. no. 381336), cleaved caspase-3 (1:1,000 dilution; cat. no. R23727), poly (ADP-ribose) polymerase (PARP; 1:1,000 dilution; cat. no. R25279) (all from ZenBio, Inc.) and GAPDH (1:2,000

dilution; cat. no. GB15004, Wuhan Servicebio Technology Co., Ltd.) were incubated with the membranes overnight at 4˚C. The second day, the membranes were washed with TBST (Wuhan Servicebio Technology Co., Ltd.) for 30 min at room temperature, and incubated with HRP-conjugated secondary antibodies (1:10,000 dilution; cat. no. C31460100, Invitrogen; Thermo Fisher Scientific, Inc.) for 1 h at room temperature. The protein expression level of each gene was detected using the ECL Pico Light Chemiluminescence kit (cat. no. SQ202, Epizyme). The gray level of each blot was measured by ImageJ software (version 1.53t, https://imagej.nih.gov/ij/, National Institutes of Health).

Immunofluorescence (IF) staining. The cells were fixed with 4% paraformaldehyde (Beyotime Institute of Biotechnology) for 30 min at room temperature and permeabilized with 0.5% Triton X-100 (Wuhan Servicebio Technology Co., Ltd.) for 30 min at room temperature, followed by blocking with 5% BSA (Wuhan Servicebio Technology Co., Ltd.) for 1 h at room temperature. FOXF1 antibody (1:500 dilution; cat. no. ab168383, Abcam, in 5% BSA) was used to incubated the cells overnight at 4˚C, followed by incubation with CoraLite594 conjugated goat anti-rabbit IgG (H+L) (1:500 dilution; cat. no. SA00013-4, Proteintech Group, Inc., in 5% BSA) for 1 h at room temperature. After mounting with Antifade Mounting Medium with DAPI (Beyotime Institute of Biotechnology), cell images were captured using an inverted confocal microscope equipped with a 400X lens objective (Zeiss AG, Germany).

Flow cytometry. Flow cytometry was used to assess the proportion of cells undergoing apoptosis. At 72 h after transfection, the cells were co-stained with Annexin V-FITC and PI (cat. no. A211; Nanjing Vazyme Biotech Co. Ltd.) according to the manufacturer's instructions. Cells with Annexin V-FITC-positive and PI-negative staining were considered to be in early stage of apoptosis, while cells with double-positive staining were considered to be in the late stage of apoptosis.

Clonogenic capacity, and Cell Counting Kit-8 (CCK-8) and 5-ethynyl-2'-deoxyuridine (EdU) assays. The cells were harvested 24 h following dsRNA transfection. For colony formation assay, 1,000 cells/well were seeded in a six-well plate with 2 ml complete medium and cultured for 10 days. The proliferating colonies were fixed with 4% paraformaldehyde (Beyotime Institute of Biotechnology) for 30 min at room temperature and stained by 0.5% crystal violet (Beyotime Institute of Biotechnology) for 2 h at room temperature. The numbers of colonies were countered using ImageJ software (version 1.53t, https://imagej.nih.gov/ij/, National Institutes of Health), and the colony formation rate was calculated as the number of colonies/1,000 cells.

A total of 5,000 cells/well were suspended in 96-well plate with 100 μl complete medium. The CCK-8 kit (1:10 dilution, 10 μl CCK-8 reagent and 90 μl complete medium per well, cat. no. C6030, NCM Biotech) was used to analyze cell growth by measuring the absorbance value at 24, 48, 72 and 96 h at 450 nm. For EdU assay, the cells were cultured with 50 μM EdU reagent (cat. no. C10310; Guangzhou Ribobio Co., Ltd.) for 2 h at 37˚C, then fixed with 4% paraformaldehyde (Beyotime Institute of Biotechnology) for 30 min at room temperature and permeabilized with 0.5% Triton X-100 (Wuhan Servicebio Technology Co., Ltd.) for 30 min at room temperature. Subsequently, the EdU-stained cells were labeled using Apollo567 reagent (Guangzhou Ribobio Co., Ltd.) for 30 min at room temperature while the cell nuclei were stained using DAPI (Wuhan Servicebio Technology Co., Ltd.) for 10 min at room temperature. Fluorescence images were captured using an inverted fluorescent microscope equipped with a 200X lens objective (Zeiss AG, Germany) and the cell proliferative ability was measured by calculating the proportion of EdU-labeled cells.

Cell migration and invasion assays. 72 h following transfection, $4x10^4$ cells were suspended in 200 μl serum-free RPMI-1640 medium and seeded into the upper chambers of a Transwell insert (24-well, 8 μm pore size, Corning, Inc.) to measure cell migration. For the invasion assay, the upper chambers were pre-coated with Matrigel (Corning, Inc., 1:5 dilution in serum-free RPMI-1640 medium). As a chemoattractant, 600 μl complete medium supplemented with 10% FBS was added to the lower chamber. The plates were cultured in incubator for 24 h at 37˚C, non-motile cells on the upper surface were removed. Following fixation with 4% paraformaldehyde (Beyotime Institute of Biotechnology; 30 min, room temperature) and staining with 0.5% crystal violet (Beyotime Institute of Biotechnology; 2 h, room temperature), the membranes were photographed under an upright fluorescent microscope microscope (x100 magnification; Zeiss AG, Germany), random fields were selected and the cell numbers were counted.

Subcutaneous xenograft tumor model. The studies involving human participants or animals were reviewed and approved by the Ethics Committee of Ruijin Hospital, School of Medicine, Shanghai Jiao Tong University (PA23030202). The animal experiments followed the ARRIVE checklist, and the animals were housed under pathogen-free, 20-26˚C, 40-70% humidity, 12-h light/dark circle conditions, with free access to water and food. The health and behavior of the animals were monitored every day; an animal would be euthanized if the length of the tumor was >17 mm. Four-week-old male BALB/c nude mice (Beijing Vital River Laboratory Animal Technology Co., Ltd.) were randomly divided into two groups (5 mice per group). EJ cells (~$6x10^6$) infected with Lenti-dsFOXF1-367 or Lenti-dsControl were dissociated into 200 μl suspension and injected subcutaneously into the right flank of each mouse. As the procedure produced only mild pain, no anesthetic was used. The length and width of the tumors were measured using calipers every 5 days, and tumor volumes were calculated as 0.5 x $width^2$ x length. All mice were sacrificed by cervical dislocation 30 days later, and after confirming that the animals had no breathing or heartbeat, the tumors were dissected for further analysis. The maximum observed tumor diameter in the animals in the present study was 7 mm.

Statistical analysis. Statistical analysis was carried out using R software (version 4.1.3; https://www.R-project.org/) and Origin 2023 software (https://www.originlab.com/). The experimental data were derived from three independent experiments

and are presented as the mean ± standard deviation (SD). For continuous variables, the Wilcoxon-Mann-Whitney (WMW) test or Student's t-test were used to examine the significance of the differences between two groups. The Kruskal-Wallis test (with Dunn's post hoc test) or one-way ANOVA (with Tukey's post hoc test) were used to determine whether or not there was a statistically significant difference among multiple groups containing non-parametric ranked data or parametric data. For categorical variables, assumptions were analyzed using the Chi-squared test or Fisher's exact test. P-value <0.05 was considered to indicate a statistically significant difference for all analyses.

Results

Patient characteristics. In the present study, 64 patients with BC that had undergone cystectomy at Ruijin hospital were recruited, 59 of them had corresponding survival information (Ruijin Cohort) and 46 of them had matched para-cancerous bladder tissues. There were 50 males and 9 females involved in this cohort, with a mean age of 68.46 years (range, 44-85 years). Their clinicopathological information was recorded and the median follow-up period was 38 months (range, 3-82 months; Tables SII and SIII). For the validation group, FOXF1 expression levels were obtained in eight GEO datasets containing tumor and normal bladder tissues, as well as in five independent BC datasets with prognostic information (IMvigor210 cohort and four GEO datasets) (23). The detailed information of these datasets is presented in Table SIV.

FOXF1 is downregulated in BC tissues. The present study aimed to explore whether FOXF1 is associated with the development of BC. FOXF1 expression was first analyzed in pan-cancer scope using TCGA database. As shown in Fig. 1A, FOXF1 expression was downregulated in numerous types of tumors. Furthermore, in BC (BLCA), FOXF1 expression exhibited a distinct difference between normal bladder and carcinoma tissues. The FOXF1 expression patterns in BC and adjacent normal tissues in the Ruijin cohort were then investigated using IHC. The staining intensity in the nuclei of the bladder tumor cells was lighter than that in the matched adjacent normal urothelial cells from T stage I to IV (Fig. S1A-H). An overview of the tissue microarray is illustrated in Fig. S1I, and the assignment of the tumor and para-cancerous tissues is presented in Fig. S1J. The H-scores of BC tissues were significantly lower than those of their matched normal bladder mucosae (P<0.001, Fig. 1B). In order to verify the universality of this downregulated FOXF1 expression in urothelial carcinoma, the FOXF1 expression levels were compared between BC tissues and normal bladder mucosae in all required GEO datasets. As shown in Fig. S2, FOXF1 expression was significantly higher in normal tissues than in BC samples (P<0.001 in GSE42089, GSE121711, GSE13507, GSE188715, GSE32864 and GSE40355; P=0.024 in GSE3167; P=0.036 in GSE37815).

Association between FOXF1 expression and the clinicopathological characteristics of patients with BC. Based on the cut-off value of H-score, the patients were divided into the FOXF1-high and FOXF1-low groups. The detailed clinicopathological information is presented in Table I. The Chi-squared test was used to examine the association between FOXF1 expression and the clinicopathological characteristics of the patients in the two groups. Compared to FOXF1-high group, FOXF1-low group had a higher proportion of patients with muscle invasion (P=0.019), worse clinical stage (P<0.001 for T stage, P<0.001 for AJCC stage) and lymphatic metastasis (P=0.011). In addition, an unfavorable survival status (P=0.003) and a shorter survival time (P=0.001) were observed in patients with a lower FOXF1 expression. There were no significant differences in sex (P=0.995), pathological grade (P=0.824) and subtype (P=0.356) between two groups (Table I). The same approach was then applied to TCGA dataset (Table SV), which contained 406 patients with BC. These results revealed that a low expression of FOXF1 was significantly associated with clinical stage (P=0.029 for AJCC stage and P<0.001 for T stage) and lymphatic metastasis (P<0.001).

Furthermore, the expression levels of FOXF1 were compared among different BC types. The FOXF1 expression level was not significantly associated with the pathological type (P=0.71, Fig. 1C) and grade (P=0.94, Fig. 1D) of BC. However, it was highly expressed in tumors without muscle invasion (P=0.026, Fig. 1E) and with early pathological stages (P=0.001 for T stage and P<0.001 for AJCC stage; Fig. 1F and G). All these results suggested that FOXF1 may exert an antitumor effect on BC.

Prognostic value of FOXF1 for the clinical outcome of patients with BC. To estimate the prognostic value of the FOXF1 expression level in the Ruijin cohort, the distribution of the H-score and survival outcomes were first evaluated. Of note, it was found that the FOXF1-high group had an improved survival rate and a longer OS (Fig. 1H and I). Furthermore, patients with high FOXF1 expression levels exhibited significantly enhanced OS than those with low FOXF1 expression levels, as determined by Kaplan-Meier analysis (P=0.00047, Fig. 1J). The mean survival time for the FOXF1-high group was 48.26 months, while for the FOXF1-low group it is 28.50 months (P=0.001, Table I).

Additionally, we attempted to verify the universality of the obtained conclusion. After screening the public databases, the following datasets were selected and analyzed to validate the predictive ability of FOXF1: TCGA-BLCA dataset, IMvigor210 cohort and four GEO datasets that contained survival data of patients with BC. In GSE48075 (P=0.011, Fig. 1K), GSE13507 (P=0.023, Fig. S3A), GSE31684 (P=0.047, Fig. S3B), IMvigor210 (P=0.043, Fig. S3C) and GSE169455 (OS: P=0.04, Fig. S3D; recurrence-free survival: P=0.037, Fig. S3E), compared with the FOXF1-low groups, the FOXF1-high groups all exhibited more favorable clinical outcomes. In TCGA dataset, to be consistent with Ruijin cohort, the OS of the patients with T2 or higher disease was compared. The patients with lower FOXF1 expression levels had poorer survival than those with higher FOXF1 expression levels, but the P-value was not significant, which might be the result of insufficient number of events and the effect of other disturbances (for instance, comorbidity or different treatment) on OS (Fig. S3F).

Subsequently, the authors examined whether FOXF1 was an independent prognostic indicator of BC. Univariate Cox regression analysis confirmed that the FOXF1 expression

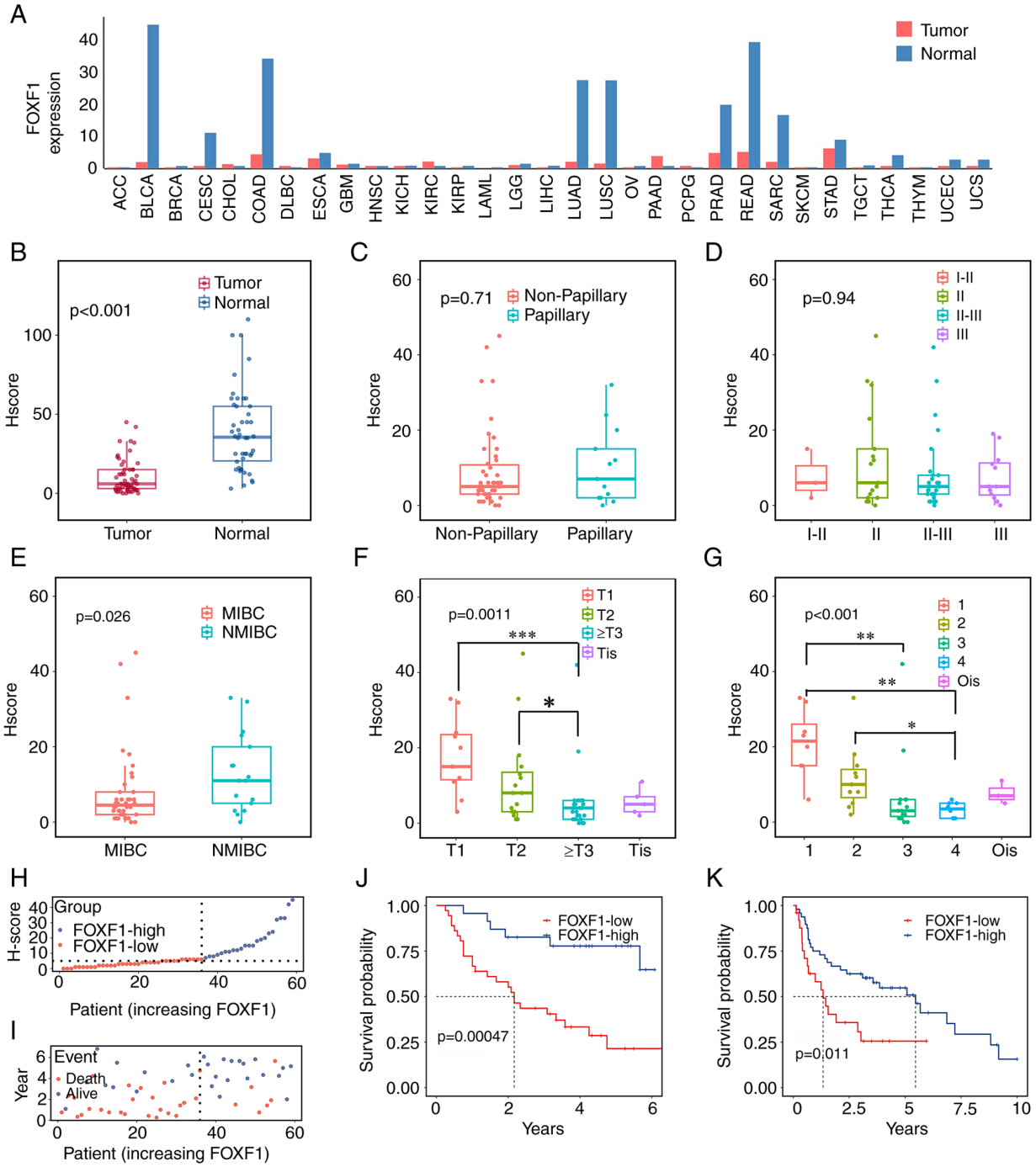

Figure 1. FOXF1 expression is downregulated in tumor tissues and is associated with a poor prognosis of patients with BC. (A) Expression of FOXF1 in pan-cancer and (B) BC tissues in the Ruijin Cohort. The association of the FOXF1 expression levels with (C) tumor type, (D) pathological grade, (E) muscle invasion, (F) T stage and (G) American Joint Committee on Cancer stage in the Ruijin Cohort. (H) The H-score curve and (I) survival status of FOXF1-low group and FOXF1-high group in the Ruijin Cohort; patients were listed in an order of increased FOXF1 expression level; the dotted line represents the cut-off value between the two groups. (J) Kaplan-Meier analysis of overall survival in the Ruijin Cohort and (K) in the GSE48075 dataset. FOXF1, forkhead box F1; BC, bladder cancer; ACC, adrenocortical carcinoma; BLCA, bladder urothelial carcinoma; BRCA, breast invasive carcinoma; CESC, cervical squamous cell carcinoma and endocervical adenocarcinoma; CHOL, cholangiocarcinoma; COAD, colon adenocarcinoma; DLBC, lymphoid neoplasm diffuse large B-cell lymphoma; ESCA, esophageal carcinoma; GBM, glioblastoma multiforme; HNSC, head and neck squamous cell carcinoma; KICH, kidney chromophobe; KIRC, kidney renal clear cell carcinoma; KIRP, kidney renal papillary cell carcinoma; LAML, acute myeloid leukemia; LGG, brain lower grade glioma; LIHC, liver hepatocellular carcinoma; LUAD, lung adenocarcinoma; LUSC, lung squamous cell carcinoma; OV, ovarian serous cystadenocarcinoma; PAAD, pancreatic adenocarcinoma; PCPG, pheochromocytoma and paraganglioma; PRAD, prostate adenocarcinoma; READ, rectum adenocarcinoma; SARC, sarcoma; SKCM, skin cutaneous melanoma; STAD, stomach adenocarcinoma; TGCT, testicular germ cell tumors; THCA, thyroid carcinoma; THYM, thymoma; UCEC, uterine corpus endometrial carcinoma; UCS, uterine carcinosarcoma.

level [hazard ratio (HR), 0.23; 95% confidence interval (CI), 0.085-0.64; P=0.0049], AJCC stage (HR, 1.9; 95% CI, 1.2-3.1; P=0.0045) and N stage (HR, 3.7, 95% CI, 1.5-9.3; P=0.0048) were significantly associated with the prognosis of patients with BC (Fig. S3G). Multivariate Cox regression analysis revealed that FOXF1 could almost predict the OS of patients

Table I. Association between FOXF1 expression and the clinicopathological characteristics of patients with BC.

Clinical features	Patients with BC	FOXF1-high	FOXF1-low	P-value
No. of patients	59	23	36	
Mean age (years), mean (SD)	68.46 (10.04)	67.83±9.81 68.86±10.30	67.58±11.01	0.703
Sex, n (%)				0.995
Male	50 (84.7)	20 (87.0)	30 (83.3)	
Female	9 (15.3)	3 (13.0)	6 (16.7)	
Stage, n (%)				<0.001
0is	3 (5.1)	2 (8.7)	1 (2.8)	
Stage i	8 (13.6)	7 (30.4)	1 (2.8)	
Stage ii	11 (18.6)	8 (34.8)	3 (8.3)	
Stage iii	15 (25.4)	2 (8.7)	13 (36.1)	
Stage iv	8 (13.6)	0 (0)	8 (22.2)	
Unknown	14 (23.7)	4 (17.4)	10 (27.8)	
Grade, n (%)				1.000
Low grade	3 (5.1)	1 (4.3)	2 (5.6)	
High grade	56 (94.9)	22 (95.7)	34 (94.4)	
Pathological grade, n (%)				
I-II	3 (5.1)	1 (4.3)	2 (5.6)	0.824
II	17 (28.8)	8 (34.8)	9 (25.0)	
II-III	27 (45.8)	9 (39.1)	18 (50.0)	
III	12 (20.3)	5 (21.7)	7 (19.4)	
Subtype, n (%)				0.356
Papillary	13 (22.0)	7 (30.4)	6 (16.7)	
Non-papillary	46 (78.0)	16 (69.6)	30 (83.3)	
Muscle invasion, n (%)				
MIBC	40 (67.8)	11 (50.0)	29 (82.9)	0.019
NMIBC	17 (28.8)	11 (50.0)	6 (17.1)	
Unknown	2 (3.4)	1 (4.3)	1 (2.8)	
Pathological T stage, n (%)				<0.001
Tis	5 (8.5)	2 (9.1)	3 (8.6)	
T1	11 (18.6)	9 (40.9)	2 (5.7)	
T2	16 (27.1)	9 (40.9)	7 (20.0)	
T3	22 (37.3)	2 (9.1)	20 (57.1)	
T4	3 (5.1)	0 (0)	3 (8.6)	
Unknown	2 (3.4)	1 (4.3)	1 (2.8)	
Pathological M stage, n (%)				/
M0	59 (100.0)	23 (100.0)	36 (100.0)	
Pathological N stage, n (%)				0.011
N0	37 (62.7)	19 (82.6)	18 (50.0)	
N1	7 (11.9)	0 (0)	7 (19.4)	
Unknown	15 (25.4)	4 (17.4)	11 (30.6)	
Survival status, n (%)				0.003
Alive	28 (47.5)	17 (73.9)	11 (30.6)	
Deceased	31 (52.5)	6 (26.1)	25 (69.4)	
Mean survival (months), mean (SD)	36.20 (22.64)	48.26 (20.13)	28.50 (20.93)	0.001

FOXF1, forkhead box F1; BC, bladder cancer; MIBC, muscle-invasive bladder cancer; NMIBC, non-muscle-invasive bladder cancer.

with BC independently (P=0.065, Fig. S3H). The aforementioned results demonstrated that the downregulated expression of FOXF1 was an unfavorable indicator of the prognosis of patients with BC; thus, it has a robust predictive ability.

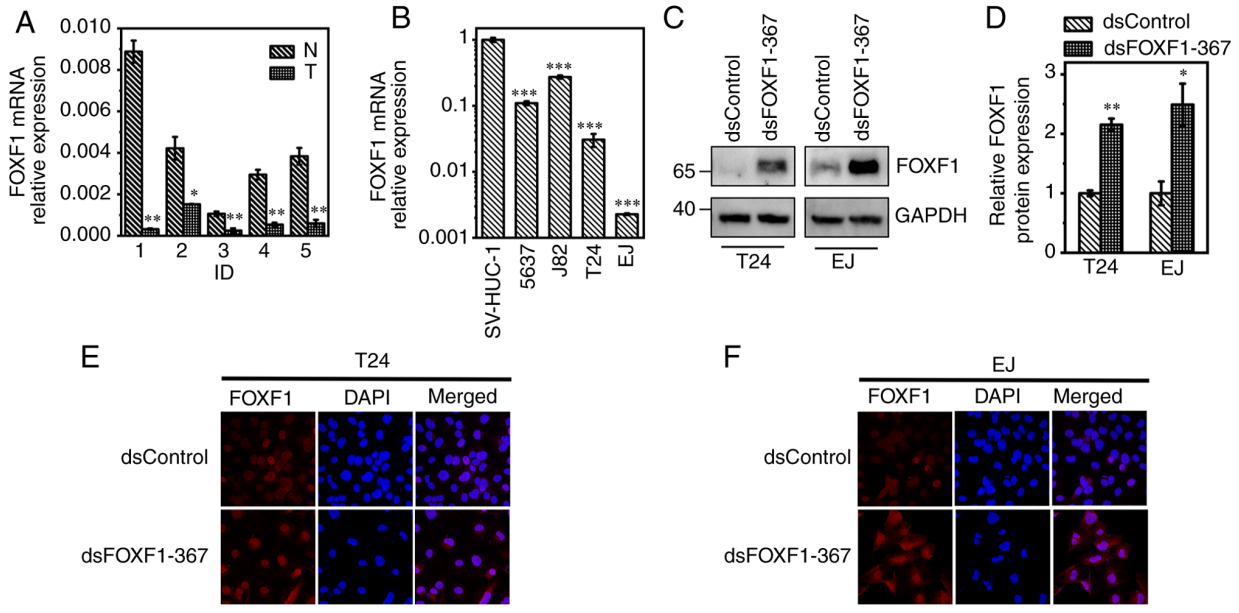

Figure 2. dsFOXF1-367 induces FOXF1 expression in human BC cells. The mRNA expression level of FOXF1 was downregulated in (A) bladder tumor tissues and (B) BC cells lines. (C) The protein expression levels of FOXF1 in T24 and EJ cells were assessed using western blot analysis; GAPDH served as the loading control; (D) the relative FOXF1 protein expression levels were quantified by determining the gray value. (E) Subcellular expression of FOXF1 protein (red) in T24 and (F) EJ cells was detected using immunofluorescence (magnification, x400); nuclei were stained with DAPI (blue). *P<0.05, **P<0.01 and ***P<0.001, vs. respective control. FOXF1, forkhead box F1; BC, bladder cancer.

Expression patterns of FOXF1 in bladder tumor specimens and cells. Following the tissue array analysis and the verification of public datasets, it was hypothesized that FOXF1 exerted a suppressive effect on BC. The analysis of the expression level of FOXF1 in 10 human bladder tissues (5 tumor specimens and 5 normal mucosae) and different cell lines revealed that FOXF1 was downregulated in bladder tumor samples and BC cells compared with para-cancerous bladder tissues and the normal uroepithelium cell line, SV-HUC-1, respectively (Fig. 2A and B).

To further investigate the antitumor role of FOXF1 in BC cells, candidate saRNAs that could activate FOXF1 expression were screened; the T24 and EJ cells were selected for use in subsequent experiments due to their lower FOXF1 expression levels, and dsControl was applied to avoid the off-target effect. Among the four designed saRNAs, dsFOXF1-367 (complementary to sequence position -367 relative to the TSS of FOXF1) led to a 5.39- and 6.85-fold induction of FOXF1 mRNA expression in the T24 and EJ cells at 72 h following transfection, respectively (Fig. S4A and B); the induction effects on FOXF1 protein expression were further compared using western blot analysis (Fig. S4C and D). According to the gray value, dsFOXF1-367 led to a 2.15- and 2.49-fold increase in FOXF1 protein levels in the T24 and EJ cells, respectively (Fig. 2C and D). IF staining also confirmed the elevated protein expression of FOXF1, and FOXF1 protein was mainly located in the cell nuclei (Fig. 2E and F).

Activation of FOXF1 expression in BC cell lines suppresses cell proliferation and induces apoptosis. First, CCK-8 assays were carried out to examine the suppressive effect of FOXF1 on BC cell proliferation (Fig. 3A and B). Compared with the dsControl, cell growth was significantly inhibited by dsFOXF1-367 from 2 days after reseeded (P<0.01, 72 h following transfection). The results of EdU assays also revealed the suppressive effects of FOXF1 on the DNA synthesis of BC cells (Fig. 3C-E). Subsequently, the growth mode of the BC cells following FOXF1 activation was examined using colony formation assay. As shown in Fig. 3F and G, FOXF1 attenuated the colony formation ability in both colony areas and colony formation rates. To determine whether FOXF1 activation affects on BC cell metastasis, Transwell assays with or without Matrigel were conducted 72 h following transfection. FOXF1 markedly suppressed cell migration (Fig. 3H) and invasion (Fig. 3I); the number of migrated and invaded cells were significantly reduced by dsFOXF1-367 (P<0.01, Fig. 3J and K).

Subsequently, flow cytometry was employed to assess the effects of FOXF1 on cell apoptosis. The induction of FOXF1 promoted both the early and late stages of apoptosis of BC cells compared with the negative control (T24 cells: Fig. 3L, M and P; EJ cells: Fig. 3N, O and Q).

FOXF1 induces the apoptosis of BC cells via the caspase signaling pathway. With the aim of elucidating the mechanisms of FOXF1 in BC cell proliferation, RNA-Seq was performed to evaluate the impact of induction on the transcriptome. T24 dsControl (nc) and T24 dsFOXF1-367 (sa) were set with three replicates of each group; 34,715 genes were differentially expressed in these two groups and 1,178 of these were protein coding genes. Through the heatmap of DEGs (Fig. 3R) and PPI (min score 65, Fig. 3S), it was noted that caspase-3 was significantly affected in the sa-vs-nc group, with $\log_2$ FC=1.27 and an adjusted P-value of 1.85×10^{-74}; in the PPI network, caspase-3 was also found as the hub gene with an interaction degree of 145 (Fig. 3T). Based on these findings, we hypothesized that FOXF1 promotes the apoptosis of BC cells via the caspase signaling pathway; this was then confirmed using western blot analysis (Fig. 3U). Furthermore,

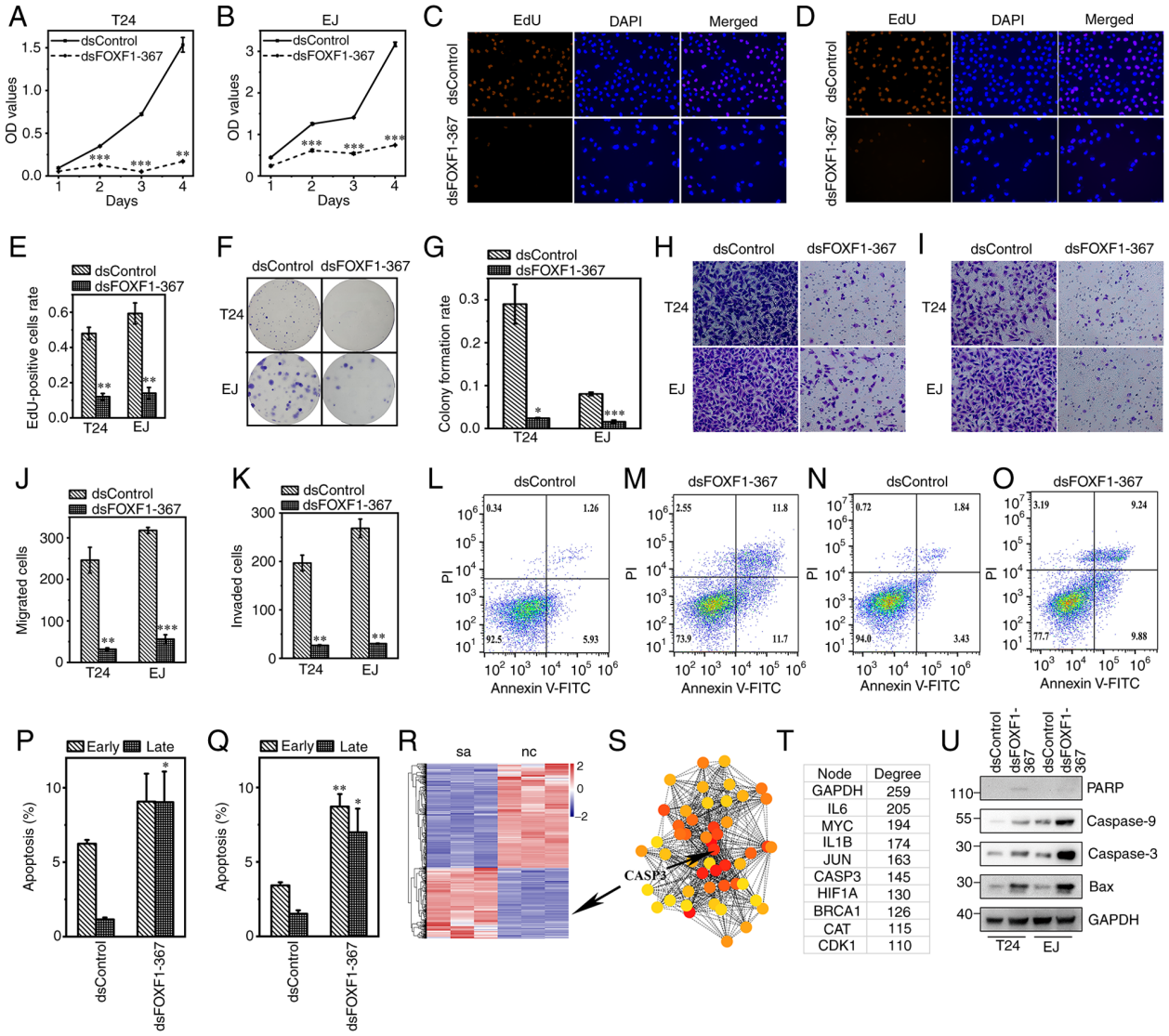

Figure 3. dsFOXF1-367 suppresses cell proliferation, migration, invasion and induces apoptosis in BC. CCK-8 assays were used to examine the viability of (A) T24 and (B) EJ cells. EdU assays revealed that dsFOXF1-367 inhibited (C) T24 and (D) EJ cell proliferation. The replicating DNA were marked with Apollo567 (orange), while nuclei were stained with DAPI (blue; magnification, x200). (E) Proportion of replication DNA in T24 and EJ cells. (F) dsFOXF1-367 impaired the clonogenic capacity of T24 and EJ cells; (G) the colony formation rate in each group was compared in the histogram. (H and I) Representative images (magnification, x200) of Transwell assays (H) with or (I) without Matrigel in T24 and EJ cells; the numbers of (J) migrated and (K) invaded cells were compared. Flow cytometry of (L and M) T24 cells following transfection with (L) dsControl or (M) dsFOXF1-367, and (N and O) EJ cells following transfection with (N) dsControl or (O) dsFOXF1-367. Percentages of (P) T24 and (Q) EJ cells in early and late apoptosis. (R) The heatmap revealed 1,178 protein coding genes among 34,715 genes which were possibly regulated by FOXF1 activation. (S) Protein-protein interaction network of potential hub genes and (T) the interaction degree of top 10 genes. (U) The protein expression levels of apoptosis-related genes. *P<0.05, **P<0.01 and ***P<0.001, vs. dsControl. FOXF1, forkhead box F1; BC, bladder cancer.

the promoting effect of FOXF1 on cell apoptosis was reversed by the inhibitor of caspase-3, and the reduced cell viability in the dsFOXF1-367-transfected groups was also recovered by this inhibitor (Fig. 4).

FOXF1 suppresses bladder tumor growth in vivo. To investigate the antitumor effects of FOXF1 *in vivo*, dsFOXF1-367 was packaged into lentivirus to construct a cell line with the stable activation of FOXF1. As dsFOXF1-367 had a more prominent activation effect in the EJ cells (Fig. S4E and F), subcutaneous xenograft tumor models were developed with Lenti-dsFOXF1-367- or Lenti-dsControl-infected EJ cells. The procedure of injection, weighting and measurements are illustrated in Fig. 5A. Lenti-FOXF1-367 impaired tumor formation; the tumor volume, weight and growth rates in the Lenti-FOXF1-367 group were significantly decreased compared with the Lenti-dsControl group (P<0.05, Fig. 5B-E). Furthermore, the volume of the xenograft models developed from Lenti-FOXF1-367 began to decline on day 25 (Fig. 5D). The mechanisms of the antitumor signaling of dsFOXF1-367 in bladder tumors are shown in Fig. 6. The antitumor effect of FOXF1 *in vitro* and *in vivo* demonstrated its promising potential in bladder cancer target therapy.

Discussion

In the present study, the downregulated expression of FOXF1 in BC tissue was revealed using IHC, and the low expression

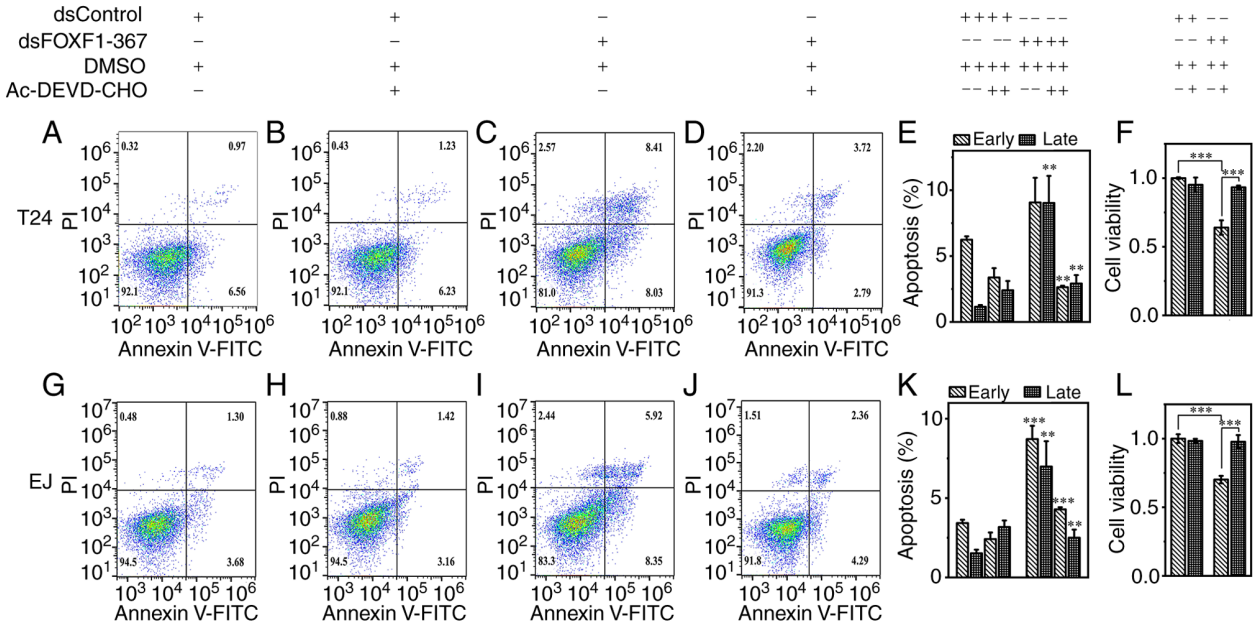

Figure 4. Promoting effect of FOXF1 on the apoptosis of T24 and EJ cells is reversed by caspase-3 inhibitor. Apoptosis assays of T24 cells treated with (A) dsControl, (B) dsControl plus caspase inhibitor, (C) dsFOXF1-367 and (D) dsFOXF1-367 plus caspase inhibitor, respectively. (E) Percentage of T24 cells undergoing apoptosis and (F) cell viability in each group. The apoptosis assays of EJ cells treated with (G) dsControl, (H) dsControl plus caspase inhibitor, (I) dsFOXF1-367 and (J) dsFOXF1-367 plus caspase inhibitor, respectively. (K) Percentage of EJ cells undergoing apoptosis and (L) cell viability in each group. **P<0.01 and ***P<0.001, vs. dsControl or as indicated. The cell apoptotic rates in the dsFOXF1-367(+) Ac-DEVD-CHO(-) groups were compared with those in the dsControl(+) Ac-DEVD-CHO(-) groups, and the cell apoptotic rates in the dsFOXF1-367(+) Ac-DEVD-CHO(+) groups were compared with those in the dsFOXF1-367(+) Ac-DEVD-CHO(-) groups, respectively. FOXF1, forkhead box F1.

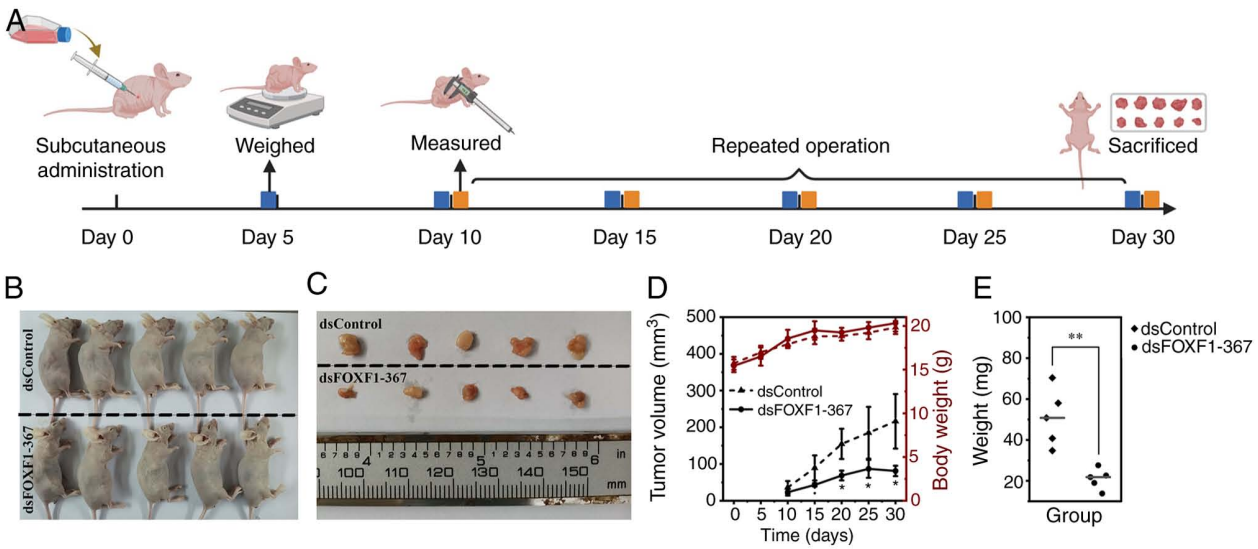

Figure 5. Activation of FOXF1 suppresses the tumorigenesis of EJ cells *in vivo*. (A) The procedure of injection, weighting and measuring of xenograft tumor models. (B) EJ Lenti-dsControl and EJ Lenti-dsFOXF1-367 cells ($6x10^6$, 200 μl) were injected into the right flanks of the mice; the mice were examined for 30 days. (C) Subcutaneous tumors in each group were dissected and photographed. (D and E) Body weights and tumor volumes in each group. *P<0.05 and **P<0.01. The image in (A) was created using BioRender.com. FOXF1, forkhead box F1.

levels were associated with more aggressive tumor phenotypes. The decreased expression of FOXF1 is an unfavorable predictor in patients with BC. The expression level of FOXF1 may be used to stratify patients with BC into groups with distinct tumor invasiveness and clinical outcomes. Moreover, the downregulated expression of FOXF1 was detected in bladder tumor samples of both Ruijin Cohort and GEO datasets. The clinical stages, invasiveness, lymphoid infiltrates and OS were significantly more severe in patients with BC with a low FOXF1 expression compared with patients with a high FOXF1 expression, confirming the stratifying ability of FOXF1. In the T24 and EJ cells, dsFOXF1-367 activated the expression level of FOXF1, this activation was dependent on the binding of the dsRNA and FOXF1 promoter sequence. FOXF1 exerted a suppressive effect on BC cells, and caspase-3 was found to be one of the downstream genes of FOXF1 through RNA seq and

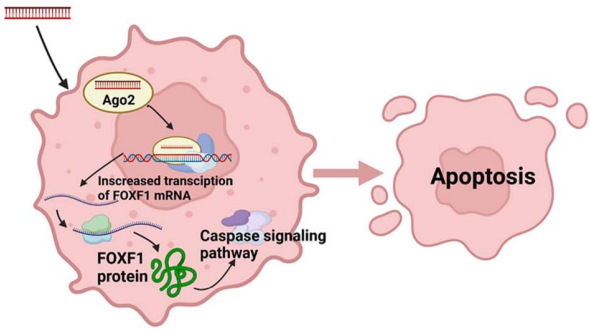

Figure 6. The mechanisms of the antitumor signaling of dsFOXF1-367 in bladder tumors. The figure was created using BioRender.com. FOXF1, forkhead box F1; Ago 2, Argonaute 2.

PPI network analyses; FOXF1 may induce BC cell apoptosis via the caspase signaling pathway.

The subcellular localization and role of FOXF1 in various types of cancers is controversial. In the present study, it was found that FOXF1-positive staining was mainly localized in the nucleus using IHC and IF staining. The nuclear expression of FOXF1 has also been found in hilar cholangiocarcinoma or metastatic pancreatic ductal adenocarcinoma (24). However, inconsistent results were observed in other types of cancer. Lo *et al* (25) revealed that FOXF1 protein was predominately expressed in the cytoplasm of epithelial cells in colorectal adenocarcinoma tissue, while positive staining was only identified in the stroma of adjacent normal tissue. Their findings illustrated that FOXF1 expression was increased and mis-localized in epithelial cells of colorectal adenocarcinoma (25).

Similar to the findings presented herein, other studies have proven that a low FOXF1 expression level is also associated with the malignant types of other tumors. In breast cancer, the increased expression of FOXF1 was shown to induce G1 phase arrest through the inactivation of the CDK2-RB-E2F cascade, thus suppressing tumor cell growth (26). In lung cancer, FOXF1 was found to be underexpressed not only in tumor samples, but also in cancer cell lines. In the manufactured FOXF1-overexpressing lung cancer cell line, the cell proliferative and migratory abilities were inhibited, accompanied by G1 phase arrest (27). In hepatocellular carcinoma, the overexpression of FOXF1 was found to impair the stemness of cancer cells, and the prognosis of patients was positively associated with the expression level of FOXF1 (16). However, Wang *et al* (28) indicated that the upregulated expression of FOXF1 was related to angiogenesis, as well as a number of aggressive clinical features in colorectal cancer (CRC). They inferred that FOXF1 could function as a promoter for the transcription of vascular endothelial growth factor A1 (VEGFA), thus altering tumor progression. In their another study, they demonstrated that the upregulation of FOXF1 expression in CRC transcriptionally elevated SNAI1 expression, promoting epithelial-mesenchymal transition by downregulating the expression level of epithelial markers (29). These studies suggest that FOXF1 might have tumor suppressor and tumor enhancer dual functions, and that it plays differential roles in various types of cancer.

FOXF1 may be a prognostic indicator in some types of cancer. In papillary thyroid cancer, the mRNA expression level of FOXF1 has been found to be significantly lower in tumor tissue than in the normal thyroid gland (15). Patients with a downregulated FOXF1 mRNA expression have been shown to have more malignant cancer phenotypes and a shorter recurrence-free survival than patients with a higher FOXF1 mRNA expression (15). Furthermore, Zhao *et al* (16) found that FOXF1 suppressed hepatocellular carcinoma *in vivo*; the FOXF1-overexpressing xenografts had lower tumor weights and PCNA expression levels than the control xenografts, and patients whose tumors had more positive FOXF1 IHC staining in the nuclei had significantly better survival outcomes than patients with a lower FOXF1 expression level (16). However, the prognostic value of FOXF1 in cancer warrants further investigation.

The caspase family consists of a number of proteolytic enzymes, their levels will culminate during apoptosis (30). According to their functions, they can be divided into two groups as follows: Initiators (includes caspase-2, -8, -9 and -10) and effectors (includes caspase-3, -6 and -7) (31,32). Caspases are usually inactive, and their activation plays a central role in the signaling pathway of apoptosis. The effector caspases (such as caspase-3) can be activated by initiator caspases (such as caspase-9) or Bax/Bak, while initiator caspases are self-activated (32,33). In the present study, the activation of FOXF1 expression induced cell apoptosis and elevated the expression level of Bax, caspase-9, caspase-3 and PARP. Moreover, the cell apoptotic rate was suppressed by caspase inhibitor. These results suggest that FOXF1 may contribute to a mitochondrial caspase-dependent apoptotic pathway in BC.

The resistance of apoptosis is a hallmark of cancer, as tumor cells are able to limit apoptosis through a number of strategies (34). However, in certain types of cancer, by regulating the tumor microenvironment, apoptosis also functions as a pro-oncogenic factor, potentiating angiogenesis, metastasis and the invasion of cancer (35). Apoptosis-driven growth and repair can stimulate the generation of the tumor microenvironment, repopulating tumors with surviving cells (36). Caspase-3 is crucial in linking the regeneration and repopulation processes. It has been reported that caspase-3 inhibitor enhances the efficacy of radiotherapy, and caspase-3 activation can predict the sensitivity of tumors to adjuvant treatment (37). This paradox of cell death may explain the ambivalent effects of FOXF1 in cancer; the 'yin and yang' of apoptosis in tumorigenesis needs further investigations.

To the best of our knowledge, the present study is the first to analyze the expression patterns, prognostic value and antitumor mechanisms of FOXF1 in BC. FOXF1 can not only strength the current staging systems, but can also assist clinical judgement. The apoptotic promoting effects of FOXF1 on BC cells suggest its potential application in tumor targeted therapy. However, there are several limitations to the present study. First, limited by the surgical quantity of cystectomy, only 59 patients were recruited in the present study. The predictive ability of FOXF1 in patients with BC remains to be validated in a larger cohort. Therefore, public datasets were utilized to validate the predictive ability of FOXF1 and its association with the clinical data of patients with BC. In TCGA dataset, 406 patients with BC were divided into the FOXF1-high and FOXF1-low groups; the patients with a higher FOXF1 expression exhibited more favorable clinicopathological features than the patients

with a lower FOXF1 expression (Table SV). Furthermore, in the GSE13507, GSE31684, GSE48075, GSE169455 and IMvigor210 cohort, patients with BC in the FOXF1-low groups all had significantly poorer survival outcomes than patients in the FOXF1-high groups (Figs. 1K and S3A-E), confirming the universality of the conclusions reached herein. Second, the present study recruited patients with BC who had undergone cystectomy, and the majority of these had high-grade urothelium carcinoma (56 out of 59 patients); thus, the expression pattern of FOXF1 in low-grade BC remains to be evaluated. Therefore, further multicenter studies with a greater number of patients and higher tumor stages are required. Third, the exact mechanisms of RNA activation, as well as the interaction between FOXF1 and caspase-3 remain unclear; thus, further studies are warranted to investigate this pathway in more detail.

In conclusion, the present study confirmed that the downregulated expression of FOXF1 was associated with unfavorable clinical stages and types in BC. FOXF1 can be used to stratify patients with BC with significantly different survival outcomes, and its expression level has a robust predictive ability as regards the prognosis of patients with BC. FOXF1 exerts antitumor effects on BC cells, as it can induce cell apoptosis in a caspase-dependent manner. This finding may be of value to staging systems, and it may assist clinical decisions for adjuvant therapies and follow-up after surgery. The activation of FOXF1 expression may be used as a novel strategy in tumor therapeutics.

Acknowledgements

Not applicable.

Funding

The present study was supported by grants from the National Natural Science Foundation of China (nos. 81602215 and 82173045) and Guangci Distinguished Young Scholars Training Program (nos. GCQN-2018-A10).

Availability of data and materials

The datasets used and/or analyzed during the current study are available from the corresponding author on reasonable request. The RNA-Seq data have been submitted to the GEO repository (accession no. GSE229810).

Authors' contributions

YH, CW and DX conceived and designed the study. YH and CW contributed to the execution of the experiments, statistical analysis of the data and in the drafting of the manuscript. WH, HW, WR, FS and YZ performed the surgeries. YH and CW confirm the authenticity of all the raw data. All authors have read and approved the final manuscript.

Ethics approval and consent to participate

The present study was performed in accordance with the Declaration of Helsinki. The studies involving human participants or animals were reviewed and approved by the Ethics Committee of Ruijin Hospital, School of Medicine, Shanghai Jiao Tong University (PA23030202). All patients/participants provided their written informed consent to participate in the study.

Patient consent for publication

Not applicable.

Competing interests

The authors declare that they have no competing interests.

References

1. Sung H, Ferlay J, Siegel RL, Laversanne M, Soerjomataram I, Jemal A and Bray F: Global cancer statistics 2020: GLOBOCAN estimates of incidence and mortality worldwide for 36 cancers in 185 countries. CA Cancer J Clin 71: 209-249, 2021.
2. Witjes JA, Bruins HM, Cathomas R, Compérat EM, Cowan NC, Gakis G, Hernández V, Espinós EL, Lorch A, Neuzillet Y, *et al*: European association of urology guidelines on muscle-invasive and metastatic bladder cancer: Summary of the 2020 guidelines. Eur Urol 79: 82-104, 2021.
3. Babjuk M, Burger M, Capoun O, Cohen D, Compérat EM, Escrig JL, Gontero P, Liedberg F, Masson-Lecomte A, Mostafid AH, *et al*: European association of urology guidelines on non-muscle-invasive bladder cancer (Ta, T1, and Carcinoma in Situ). Eur Urol 81: 75-94, 2022.
4. de Oliveira MC, Caires HR, Oliveira MJ, Fraga A, Vasconcelos MH and Ribeiro R: Urinary biomarkers in bladder cancer: Where do we stand and potential role of extracellular vesicles. Cancers (Basel) 12: 1400, 2020.
5. Allory Y, Beukers W, Sagrera A, Flández M, Marqués M, Márquez M, van der Keur KA, Dyrskjot L, Lurkin I, Vermeij M, *et al*: Telomerase reverse transcriptase promoter mutations in bladder cancer: High frequency across stages, detection in urine, and lack of association with outcome. Eur Urol 65: 360-366, 2014.
6. Moonen PM, Kiemeney LA and Witjes JA: Urinary NMP22 bladderchek test in the diagnosis of superficial bladder cancer. Eur Urol 48: 951-956, 2005.
7. Lam EWF, Brosens JJ, Gomes AR and Koo CY: Forkhead box proteins: Tuning forks for transcriptional harmony. Nat Rev Cancer 13: 482-495, 2013.
8. Katoh M, Igarashi M, Fukuda H, Nakagama H and Katoh M: Cancer genetics and genomics of human FOX family genes. Cancer Lett 328: 198-206, 2013.
9. Yamashita H, Amponsa VO, Warrick JI, Zheng Z, Clark PE, Raman JD, Wu XR, Mendelsohn C and DeGraff DJ: On a FOX hunt: Functions of FOX transcriptional regulators in bladder cancer. Nat Rev Urol 14: 98-106, 2017.
10. Katoh M and Katoh M: Human FOX gene family (Review). Int J Oncol 25: 1495-1500, 2004.
11. Mahlapuu M, Ormestad M, Enerback S and Carlsson P: The forkhead transcription factor Foxf1 is required for differentiation of extra-embryonic and lateral plate mesoderm. Development 128: 155-166, 2001.
12. Paulsson J and Micke P: Prognostic relevance of cancer-associated fibroblasts in human cancer. Semin Cancer Biol 25: 61-68, 2014.
13. Sturtzel C, Lipnik K, Hofer-Warbinek R, Testori J, Ebner B, Seigner J, Qiu P, Bilban M, Jandrositz A, Preisegger KH, *et al*: FOXF1 mediates endothelial progenitor functions and regulates vascular sprouting. Front Bioeng Biotechnol 6: 76, 2018.
14. Ren X, Ustiyan V, Pradhan A, Cai Y, Havrilak JA, Bolte CS, Shannon JM, Kalin TV and Kalinichenko VV: FOXF1 transcription factor is required for formation of embryonic vasculature by regulating VEGF signaling in endothelial cells. Circ Res 115: 709-720, 2014.
15. Gu Y and Hu C: Bioinformatic analysis of the prognostic value and potential regulatory network of FOXF1 in papillary thyroid cancer. Biofactors 45: 902-911, 2019.

16. Zhao ZG, Wang DQ, Hu DF, Li YS and Liu SH: Decreased FOXF1 promotes hepatocellular carcinoma tumorigenesis, invasion, and stemness and is associated with poor clinical outcome. Onco Targets Ther 9: 1743-1752, 2016.
17. Herrera-Merchan A, Cuadros M, Rodriguez MI, Rodriguez S, Torres R, Estecio M, Coira IF, Loidi C, Saiz M, Carmona-Saez P and Medina PP: The value of lncRNA FENDRR and FOXF1 as a prognostic factor for survival of lung adenocarcinoma. Oncotarget 11: 1172-1185, 2020.
18. Magers MJ, Lopez-Beltran A, Montironi R, Williamson SR, Kaimakliotis HZ and Cheng L: Staging of bladder cancer. Histopathology 74: 112-134, 2019.
19. Davis S and Meltzer PS: GEOquery: A bridge between the gene expression omnibus (GEO) and bioconductor. Bioinformatics 23: 1846-1847, 2007.
20. Zeng D, Ye Z, Shen R, Yu G, Wu J, Xiong Y, Zhou R, Qiu W, Huang N, Sun L, *et al*: IOBR: Multi-omics immuno-oncology biological research to decode tumor microenvironment and signatures. Front Immunol 12: 687975, 2021.
21. Huang V, Qin Y, Wang J, Wang X, Place RF, Lin G, Lue TF and Li LC: RNAa is conserved in mammalian cells. PLoS One 5: e8848, 2010.
22. Livak KJ and Schmittgen TD: Analysis of relative gene expression data using real-time quantitative PCR and the the 2(-Delta Delta C(T)) method. Methods 25: 402-408, 2001.
23. Hoffman-Censits JH, Grivas P, Van Der Heijden MS, Dreicer R, Loriot Y, Retz M, Vogelzang NJ, Perez-Gracia JL, Rezazadeh A, Bracarda S, *et al*: IMvigor 210, a phase II trial of atezolizumab (MPDL3280A) in platinum-treated locally advanced or metastatic urothelial carcinoma (mUC). J Clin Oncol 34 (Suppl 2): S355, 2016.
24. Hrudka J, Prouzová Z, Mydlíková K, Jedličková K, Holešta M, Whitley A and Havlůj L: FOXF1 as an immunohistochemical marker of hilar cholangiocarcinoma or metastatic pancreatic ductal adenocarcinoma. Single institution experience. Pathol Oncol Res 27: 1609756, 2021.
25. Lo PK, Lee JS, Chen H, Reisman D, Berger FG and Sukumar S: Cytoplasmic mislocalization of overexpressed FOXF1 is associated with the malignancy and metastasis of colorectal adenocarcinomas. Exp Mol Pathol 94: 262-269, 2013.
26. Lo PK, Lee JS, Liang X, Han L, Mori T, Fackler MJ, Sadik H, Argani P, Pandita TK and Sukumar S: Epigenetic inactivation of the potential tumor suppressor gene FOXF1 in breast cancer. Cancer Res 70: 6047-6058, 2010.
27. Wu CY, Chan CH, Dubey NK, Wei HJ, Lu JH, Chang CC, Cheng HC, Ou KL and Deng WP: Highly expressed FOXF1 inhibit non-small-cell lung cancer growth via inducing tumor suppressor and G1-phase cell-cycle arrest. Int J Mol Sci 21: 3227, 2020.
28. Wang S, Xiao Z, Hong Z, Jiao H, Zhu S, Zhao Y, Bi J, Qiu J, Zhang D, Yan J, *et al:* FOXF1 promotes angiogenesis and accelerates bevacizumab resistance in colorectal cancer by transcriptionally activating VEGFA. Cancer Lett 439: 78-90, 2018.
29. Wang S, Yan S, Zhu S, Zhao Y, Yan J, Xiao Z, Bi J, Qiu J, Zhang D, Hong Z, *et al*: FOXF1 induces epithelial-mesenchymal transition in colorectal cancer metastasis by transcriptionally activating SNAI1. Neoplasia 20: 996-1007, 2018.
30. Creagh EM, Conroy H and Martin SJ: Caspase-activation pathways in apoptosis and immunity. Immunol Rev 193: 10-21, 2003.
31. Van Opdenbosch N and Lamkanfi M: Caspases in cell death, inflammation, and disease. Immunity 50: 1352-1364, 2019.
32. Shi Y: Mechanisms of caspase activation and inhibition during apoptosis. Mol Cell 9: 459-470, 2002.
33. Vince JE, De Nardo D, Gao W, Vince AJ, Hall C, McArthur K, Simpson D, Vijayaraj S, Lindqvist LM, Bouillet P, *et al*: The mitochondrial apoptotic effectors BAX/BAK activate caspase-3 and -7 to trigger NLRP3 inflammasome and caspase-8 driven IL-1β activation. Cell Rep 25: 2339-2353.e4, 2018.
34. Hanahan D and Weinberg RA: Hallmarks of cancer: The next generation. Cell 144: 646-674, 2011.
35. Ford CA, Petrova S, Pound JD, Voss JJ, Melville L, Paterson M, Farnworth SL, Gallimore AM, Cuff S, Wheadon H, *et al*: Oncogenic properties of apoptotic tumor cells in aggressive B cell lymphoma. Curr Biol 25: 577-588, 2015.
36. Morana O, Wood W and Gregory CD: The apoptosis paradox in cancer. Int J Mol Sci 23: 11328, 2022.
37. Huang Q, Li F, Liu X, Li W, Shi W, Liu FF, O'Sullivan B, He Z, Peng Y, Tan AC, *et al*: Caspase 3-mediated stimulation of tumor cell repopulation during cancer radiotherapy. Nat Med 17: 860-866, 2011.